Received August 12, 2020, accepted August 27, 2020, date of publication September 9, 2020, date of current version October 16, 2020.

Digital Object Identifier 10.1109/ACCESS.2020.3022845

A Compact Dual Circularly Polarized Antenna With Wideband Operation and High Isolation

HUY HUNG TRAN[1,2], NGHIA NGUYEN-TRONG[3], (Member, IEEE), AND HYUN CHANG PARK[4], (Member, IEEE)

[1]Division of Computational Physics, Institute for Computational Science, Ton Duc Thang University, Ho Chi Minh City 758307, Vietnam
[2]Faculty of Electrical and Electronics Engineering, Ton Duc Thang University, Ho Chi Minh City 758307, Vietnam
[3]School of ITEE, The University of Queensland, Brisbane, QLD 4072, Australia
[4]Division of Electronics and Electrical Engineering, Dongguk University, Seoul 100-715, South Korea

Corresponding author: Hyun Chang Park (hcpark@dongguk.edu)

ABSTRACT This paper presents a dual-sense circularly polarized (CP) antenna with compact size, high isolation, and wideband characteristics. The antenna consists of a microstrip patch, an array of parasitic metal plates positioned around the patch, and a 90° branch line coupler as feeding structure. Unlike the conventional design method, we demonstrate that the wide isolation bandwidth can be achieved with an imperfect coupler and imperfect matching at the radiating element. The final design with overall dimensions of $0.59\lambda_c \times 0.59\lambda_c \times 0.06\lambda_c$ (λ_c is the free-space wavelength at center operating frequency) was fabricated and tested. Measurements on the fabricated prototype show that the antenna has a bandwidth of 16.5% (5.0–5.9 GHz) with port isolation of better than 15 dB. In addition, a peak broadside gain of about 6.6 dBic is attained. In comparison with other related works in literature, this antenna has advantages of wide operating bandwidth with high isolation while possessing a compact footprint.

INDEX TERMS Circular polarization, dual polarization, patch antenna, wideband, high isolation.

I. INTRODUCTION

Dual circularly polarized (CP) antennas are particularly useful for miniaturized systems with polarization diversity or frequency reuse [1]. This type of antenna can find various applications such as satellite communication, radio frequency identification (RFID), MIMO systems, etc. Owing to the merits of low profile, light weight, and ease of fabrication, the slot or the loop antenna is a popular choice in realizing dual CP polarizations [2]–[6]. However, these types of antennas are featured by bi-directional radiation pattern. For applications requiring unidirectional beam, various designs based on the low-profile microstrip patch structure have been reported. Patch antennas fed by two L-strips [7] or a coplanar waveguide transmission line [8] were able to produce dual-CP radiation with 3-dB axial ratio (AR) bandwidth (BW) of less than 5%. Better performance can be achieved by feeding the square patch with multiple slots [9], [10], a suspended strip line [11] or U-shaped slots [12]. Alternatively, techniques using a metasurface [13], [14] or a substrate integrated waveguide [15], [16] have also been demonstrated as promising candidates for low-profile, wideband, dual-CP antenna. However, most of the above-mentioned designs suffer from narrow operating BW, typically less than 15%. Besides, they also possess other drawbacks such as using a large footprint or complicated feeding structures.

In the open literature, many designs have utilized a branch line coupler as an effective method to achieve dual circular polarization [17]–[22]. The coupler ensures having two output signals equal in magnitude with 90° phase shift needed for CP generation. Using a hybrid coupler as feeding structure, the antenna can provide either left-hand CP (LHCP) or right-hand CP (RHCP) depending on the excited port. Although wide AR BW can be conveniently accomplished in [17]–[22] by this method, the most challenging aspect is the poor inter-port isolation. The literature review has found that the best performance in the operating BW is only about 15% [17] with isolation of better than 15 dB, where the radiating patch is coupled to the coupler through double H-shaped slots. Meanwhile, the limited BW with high isolation in the designs in [18]–[22] might not be particularly appealing for wideband applications.

This paper presents a design of dual-CP antenna, which is able to provide a good isolation of better than 15 dB over a wide frequency band of 16.5%. The method of using a branch line coupler to excite a square microstrip patch for dual-sense

The associate editor coordinating the review of this manuscript and approving it for publication was Jaime Laviada.

CP operation is employed. However, unlike the conventional designs [17]–[21] in which the coupler is separated from the radiating elements by the ground plane, the coupler in the proposed design is positioned between the radiating element and the ground plane. Additionally, a set of metallic plates is also placed periodically around the driven patch and acts as parasitic elements, which provide more degrees of freedom in optimizing the antenna performance for a wide BW. Notably, we will demonstrate that a large isolation BW can be achieved with an imperfect feeding coupler and imperfect matching at the radiating patch.

II. DESIGN GEOMETRY

A. CONVENTIONAL DESIGN

Fig. 1 shows the diagram of the dual-sense CP antenna using conventional design method. When the coupler is designed to be perfect, the two output ports (Port 3 and Port 4) will have equal magnitude and 90° phase difference. If the patch is well matched at Port 3 and Port 4, excellent CP operation will be achieved with the rotating sense depending on the feeding port (Port 1 or Port 2). Moreover, for a perfect coupler, the power coupled to Port 2 is extremely small, yielding high isolation. The design procedure for this antenna type has been clearly described in [19] and not shown here for brevity. The most essential disadvantage of this classical configuration is the limited isolation BW due to the fact that the coupler typically has narrow BW. The other technical drawback is that the coupler often takes up a large space, which increases the overall size. To overcome this, the coupler is placed on a substrate below the ground plane. This method has been applied on most reported papers in literature [17]–[21]. Nevertheless, this configuration still takes up some space below the antenna structure while this space might be necessary for other microwave circuits.

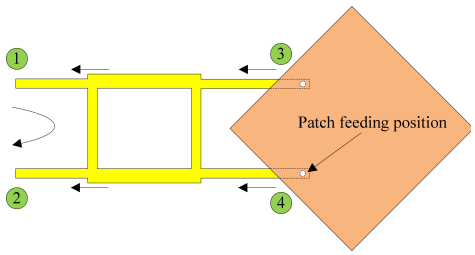

FIGURE 1. Geometry of the conventional dual-CP antenna with coupler.

B. PROPOSED SOLUTION

To solve the abovementioned disadvantages, we present a solution shown in Fig. 2. In this particular design, the antenna is patterned on two 1.52-mm-thick Taconic RF-35 substrates with dielectric constant $\varepsilon = 3.5$ and loss tangent $\tan\delta = 0.0018$. Unlike the conventional designs [17]–[21], the branch line coupler is placed in between the ground plane and the radiating patch, and directly stacked under the driven patch. It is noted that in this proposed design, the coupler acts as a feeding structure that is integrated into the overall

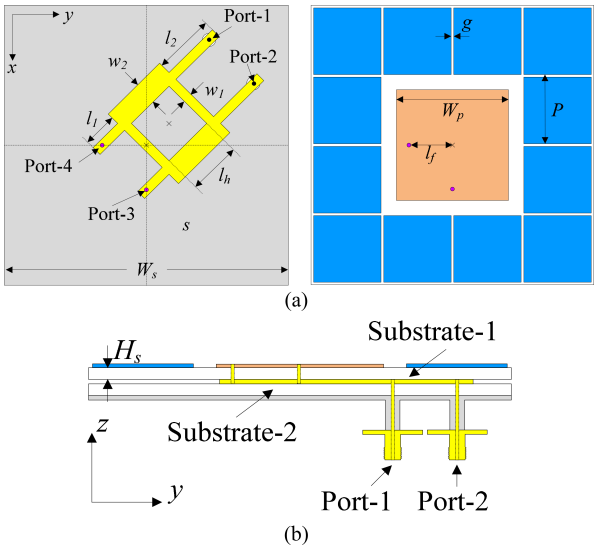

FIGURE 2. Geometry of the proposed dual-CP antenna: (a) top view, (b) side view.

antenna structure. This contributes to the miniaturization of the antenna's footprint. For antenna testing, coaxial connectors are used to excite the two input ports (Port 1 and Port 2) as demonstrated in Fig. 2. Here, no extra circuit is required below the ground. Finally, to provide more degree of freedom in optimizing the antenna characteristics (with a trade-off in overall antenna dimensions), an array of 12 square metallic plates is arranged periodically around the driven patch.

The antenna was characterized using the ANSYS high-frequency structure simulator (HFSS) and the optimized geometrical parameters were chosen as follows: $W_s = 32$, $H_s = 1.52$, $W_p = 12.8$, $l_f = 5$, $P = 8$, $g = 0.3$, $w_1 = 1.1$, $w_2 = 2.6$, $l_1 = 3.9$, $l_2 = 6.9$, $l_h = 6$ (unit: mm).

III. DESIGN MOTIVATION AND OPERATION PRINCIPLE

This section will explain the motivation and principle to construct the design as shown in Fig. 2. First, our ultimate goal is to obtain a dual-sense CP antenna with wideband characteristics. This means we need to achieve a structure that can exhibit wide impedance matching BW, wide isolation BW and wide AR BW at the same time. For wide AR BW, two orthogonal modes with about 90° phase difference and the same magnitude are required to be excited in a wide range of frequency. This is achieved by using a hybrid coupler feed. In theory, a lossless passive symmetrical directional coupler should exhibit about 90° phase shift in a wide BW as long as the isolation and matching are reasonable [23]. This is the main reason why most of the designs using coupler as feeding can obtain a wide AR BW [17]–[22]. For wide impedance matching, a substrate with high thickness is preferred, thus we choose $H_s = 1.52$ mm, so the total thickness is 3.04 mm (about $0.055\lambda_c$ where λ_c is the free-space wavelength at the center frequency of 5.5 GHz). In fact, the most challenging issue in this design is to obtain a wide isolation BW since the criterion for isolation is stricter than that for impedance

matching (e.g. typically better than 15 dB or 20 dB). The principle to achieve this is explained in the following.

Let $\left[S_{ij}^c\right]$ be the S-parameters of the coupler in Fig. 1. Let us consider an excitation with unit amplitude at Port 1. At first, there will be a small level of power travelling to Port 2, corresponding to S_{21}^c (if the coupler has perfect isolation, then $S_{21}^c = 0$). Other parts of RF power travel to Port 3 and Port 4. The antenna acts as a load with impedance $Z_L = Z_{ant}$. When Z_{ant} is not perfectly matched to the characteristic impedance at Port 3 and Port 4 of the coupler, there will be a reflection, which is indicated by Γ_a where Γ_a is the reflection coefficient of the antenna alone (without coupler feeding). It is noted that Γ_a is similar at Port 3 and Port 4 due to the symmetry of the structure. These reflections will travel back to Port 2 through the coupler and contribute to the overall S_{21} of the whole device. Therefore, the coupling between Port 1 and Port 2 of the whole antenna can be estimated as:

$$S_{21} \approx S_{21}^c + S_{31}^c \Gamma_a S_{23}^c + S_{41}^c \Gamma_a S_{24}^c (1) \quad (1)$$

If the coupler is symmetrical, $S_{31}^c = S_{24}^c$ and $S_{23}^c = S_{41}^c$. Thus, (1) can be rewritten as:

$$S_{21} \approx S_{21}^c + 2S_{31}^c S_{23}^c \Gamma_a (2) \quad (2)$$

As for the conventional approach, high isolation ($S_{21} = 0$) is achieved by enforcing both conditions $S_{21}^c = 0$ and $\Gamma_a = 0$, i.e. the coupler has perfect isolation and antenna has perfect matching at its feeding position. These two strict requirements result in a narrow isolation BW [18]–[22]. However, equation (2) indicates that for $S_{21} = 0$, it is not necessary to have both conditions satisfied. In fact, S_{21} can be zero as long as the two operands in (2) have the *same magnitude* and *opposite phase*. It is found through various simulations with the coupler alone that S_{21}^c can be designed to be in the range of about -10 to -15 dB in a wide range of frequency. The value of $2S_{31}^c S_{23}^c$ is exactly 1 if the coupler is perfect. For the imperfect coupler under consideration, the value of $2S_{31}^c S_{23}^c$ can be about -2 dB to -3 dB. Thus, the antenna should be designed to have Γ_a around -7 dB to -12 dB (when there is no coupler). This can be achieved by optimizing the patch and the parasitic elements' dimensions. The interesting point here is that the phase of $2S_{31}^c S_{23}^c \Gamma_a$ can be easily controlled (without affecting phase of S_{21}^c) by varying the length at the output ports (l_1) so that it can provide an opposite phase to S_{21}^c.

Based on the above explanation, it can be concluded that a high isolation between Port 1 and Port 2 can be achieved with an imperfect coupler and imperfect matching at antenna feeding position. The improvement in the isolation is due to the cancellation in different coupling paths as shown in equation (2). This condition is not as strict as in conventional approach, i.e. $S_{21}^c = 0$ and $\Gamma_a = 0$, providing more degrees of freedom in antenna optimization. Therefore, it is possible to achieve a wider isolation BW in this design. For demonstration, Fig. 3 shows the S-parameter for the coupler alone, antenna alone (without coupler) and the final optimized design. It can be observed that both the coupler and the antenna matching are highly imperfect. However, a wide isolation BW can be achieved in the final design.

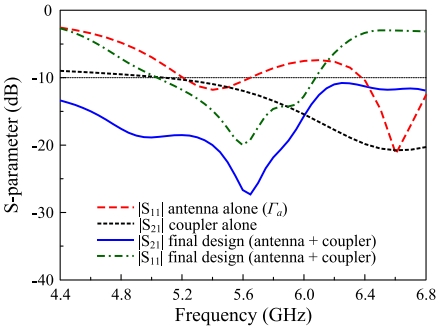

FIGURE 3. S-parameter of the antenna alone, the coupler alone, and the final design. The target frequency range is from 5.0 GHz to about 6.0GHz.

IV. KEY PARAMETER STUDY AND DESIGN PROCEDURE

It has to be clarified here that equations (1) and (2) only serve to demonstrate the principle of achieving low $|S_{21}|$ without having perfect coupler feeding and antenna matching (Γ_a). In practice, since the coupler is placed in between the ground plane and the radiating elements, the operation of the coupler is affected by the patches and parasitic elements. Moreover, the radiating modes of the patch are affected by the coupler and there is also a direct coupling between two antenna ports. Thus, the antenna optimization is quite complicated. In order to provide the readers a comprehensive design procedure, several key parameter studies will be demonstrated in this section. The target operating bandwidth for investigation is from 5.0 to about 6.0 GHz.

A. KEY PARAMETER STUDY

The first important parameters are related to the parasitic elements, including the gap (g) and the periodicity (P). It is noted that the parasitic elements provide more degree of freedom and also play a critical role in optimizing the operating BW and isolation characteristics of the proposed design. Fig. 4 shows the antenna features for different values of g. First, it can be seen that g has minor effect on the overall impedance matching while the isolation and the AR are significantly affected. This is because the gap g primarily controls the coupling between these parasitic patches. These extra couplings can be superimposed with the existing coupling between two ports and thus affects S_{21}. Additionally, the gap g has effect on the two orthogonal modes, and therefore can be used to optimize the AR. Fig. 5 shows the phase difference and amplitude of two orthogonal modes, which are obtained by using the polarization ratio function in HFSS. As observed, while the phase difference remains around 90° in all cases, the relative amplitude of two orthogonal modes can be controlled with the value of g. Although the antenna is completely symmetric with respect to the two feed points, when only one port is excited, the structure is asymmetry with respect to that port. Therefore, it is expected that varying gap

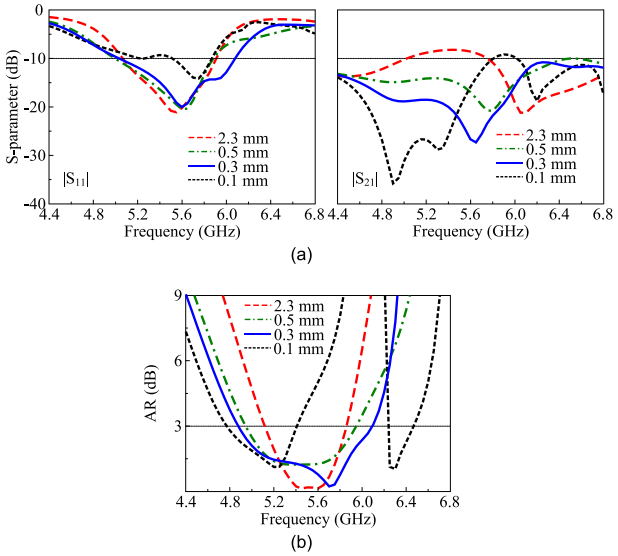

FIGURE 4. Simulated (a) S-parameter and (b) AR of the proposed antenna for different *g*.

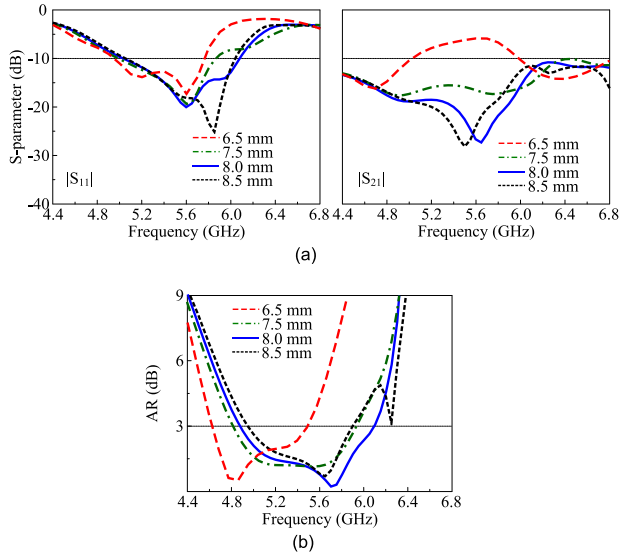

FIGURE 6. Simulated (a) S-parameter and (b) AR of the proposed antenna for different *P*.

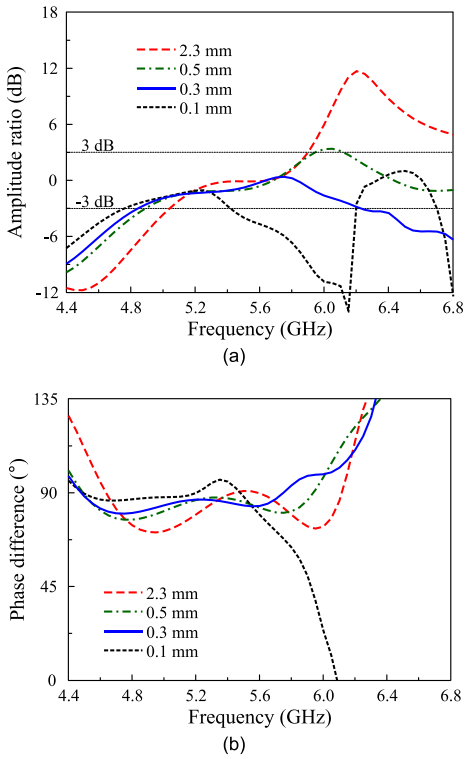

FIGURE 5. Simulated (a) amplitude ratio and (b) phase difference of two orthogonal fields of the proposed antenna for different *g*.

g will have an effect on the two orthogonal modes and AR performance. It should be clarified here that this mechanism is different from what is explained in Section III. In fact, it provides additional degree of freedom to optimize for the BW. Through various numerical simulations, we found that for the target frequency range, an appropriate value of *g* is about 0.3 mm.

Fig. 6 shows the results with different values of P while keeping g at 0.3 mm. In general, the optimization will be more difficult with smaller value of P and the operating BW is degraded for more compact structure. In the proposed design, P is chosen so that the antenna size is minimized while maintaining reasonable operating features ($P = 8$ mm). The total antenna size is $0.59\lambda_c \times 0.59\lambda_c$.

In order to tune the performance of S_{21} according to equation (2), we can tune the length l_1, which controls the phase of S_{31}^c and S_{23}^c. Fig. 7 shows the antenna characteristics for different values of l_1. As expected, a wide AR BW is still reasonably achieved as the phase difference between two orthogonal modes is maintained around 90° with a symmetrical hybrid coupler. Most of the changes in AR are due to the fact that when l_1 varies, the position of Port 1 and Port 2 also changes which affects some extra direct coupling from the feed to the parasitic patches. Meanwhile, S_{21} is strongly affected by l_1. In fact, using the same analytical approach as in Section 2, it can be easily shown that $|S_{11}|$ should also be affected by the length l_1. However, since the criterion for S_{11} is typically not as strict as S_{21}, i.e. $|S_{11}| < -10$ dB while $|S_{21}|$ should be as low as possible, it is found that in most cases, the changes in $|S_{11}|$ is acceptable.

B. DESIGN PROCEDURE

Based on the above key parameter studies, the design procedure of the proposed antenna can be summarized as follows:

Step 1: Design an imperfect coupler as feeding structure with isolation around 10 to 15 dB across the bandwidth. This can be achieved by tuning w_1, w_2 ($w_2 > w_1$) and l_h(initially around quarter effective-wavelength). The initial value for w_1 can be chosen such that the impedance for the w_1 -line is about 50 Ω (Note that the performance of this coupler is not critical at this stage).

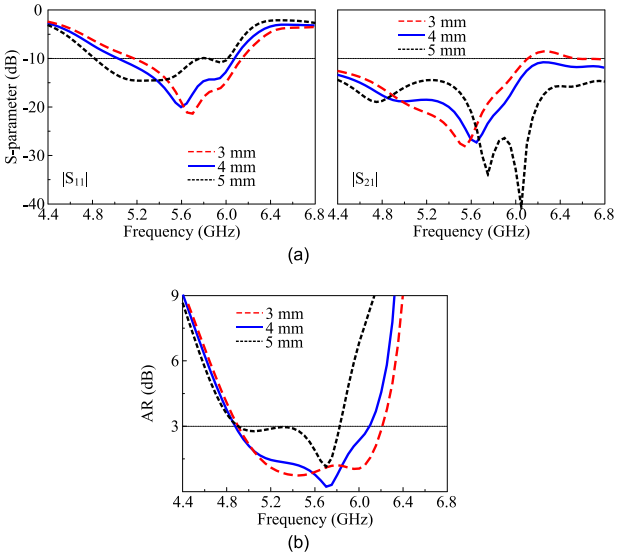

FIGURE 7. Simulated (a) S-parameter and (b) AR of the proposed antenna for different l_1.

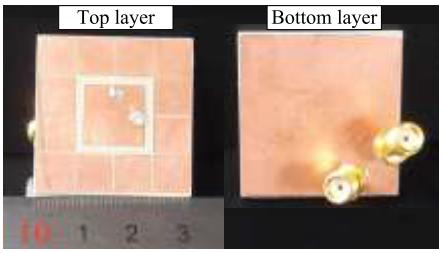

FIGURE 8. Photographs of the fabricated dual-CP antenna.

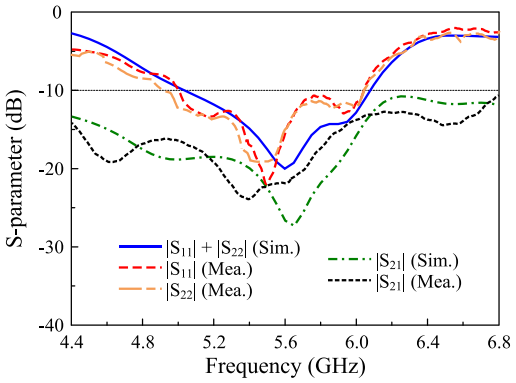

FIGURE 9. Simulated and measured S-parameter of the proposed dual-CP antenna.

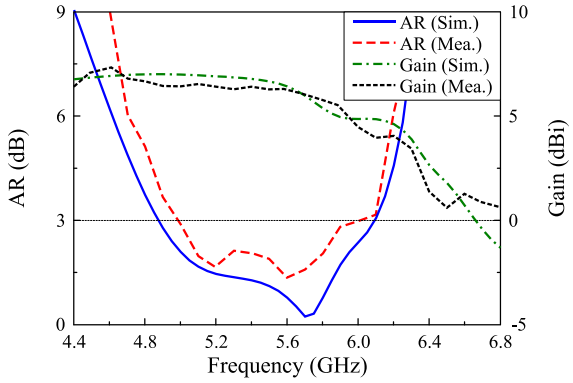

FIGURE 10. Simulated and measured AR and gain at broadside direction of the proposed dual-CP antenna.

Step 2: Design the square patch (W_p). The patch operates in the fundamental TM_{01} mode and thus, W_p is chosen about half-effective-wavelength at the center frequency.

Step 3: Design the parasitic elements with periodicity P and gap g. P is chosen so that the antenna size is compact enough with satisfactory performance. It is empirically found that for this design, P should be chosen to have an overall antenna size of about $0.6\lambda_c$. Then, tune g to have good antenna performances in terms of AR BW and isolation.

Step 4: Tune l_1 to have the best isolation characteristics in the operating BW. Fine-tune all other parameters to improve the performance.

V. MESUREMENT RESULTS

The antenna was fabricated to validate the proposed concept. The photographs of fabricated prototype are shown in Fig. 8. In our design, when Port 1 is excited, the antenna radiates LHCP waves in the broadside direction. In contrast, if the feeding is applied to Port 2, RHCP is obtained. It is also noted that due to the symmetry, the antenna working in either RHCP or LHCP states has very similar return loss. Therefore, only the far-field measurements with Port 1 excitation are demonstrated here.

Figs. 9 and 10 present the simulated and measured S-parameters, AR, as well as broadside gain of the proposed antenna. The antenna has measured operating BW of 16.5% (5.0–5.9 GHz), in which $|S_{11}|$ is less than –10 dB, $|S_{21}|$ is below –15 dB, and the AR is lower than 3 dB. Across this band, the measured gain ranges from 4.3 to 6.6 dBic. Additionally, the operating BW of the proposed antenna with isolation of better than 20 dB is about 8.9% (5.23–5.72 GHz). It should be noted that the cancellation in the two coupling paths shown in equations (1) and (2) does not affect the antenna efficiency. Since no resistive or active component is used, the antenna is expected to have high efficiency. In fact, the simulated efficiency is better than 95% across the BW of 16.5%. Furthermore, a good agreement between the simulated and measured gains also indicates a high practical efficiency. Fig. 11 plots the gain radiation patterns of the proposed antenna at 5.2 and 5.8 GHz in two principle planes of x-z and y-z. It can be seen that RHCP radiation is dominant when Port 1 is excited. Furthermore, the polarization isolation in the broadside direction is always better than 15 dB across the operating BW. It is noted that the patterns are slightly titled due to the effect of the coupler, which causes a non-uniform field distribution on the patch and parasitic elements. Nevertheless, the gain deviation between the broadside and

TABLE 1. Performance comparison among dual-CP antennas.

Ref.	Overall size (λ_c)	Substrate dielectric constant	Coupler	AR BW (%)	Operating BW (%)		Peak gain (dBic)
					15 dB isolation	20 dB isolation	
[9]	0.96 × 0.96 × 0.20	2.5	No	16.0	9.3	6.1	9.6
[10]	0.39 × 0.39 × 0.04	4.4	No	11.0	5.9	< 3.0	4.9
[11]	0.83 × 0.83 × 0.12	4.3	No	25.1	8.0	< 3.0	7.8
[12]	0.72 × 0.72 × 0.09	2.2	No	11.5	18.5	7.6	7.9
[13]	0.73 × 0.73 × 0.07	4.4	No	12.4	12.4	9.7	7.1
[14]	0.85 × 0.85 × 0.05	3.5	No	31.3	14.0	< 3.0	7.0
[17]	0.76 × 0.76 × 0.07	4.4	Yes	N/A	~15.0	7.8	6.2
[21]	0.77 × 0.77 × 0.22	2.2	Yes	< 3.0	7.8	< 3.0	4.9
[22]	0.50 × 0.50 × 0.06	3.4	Yes	< 3.0	1.0	< 3.0	7.5
Prop.	0.59 × 0.59 × 0.06	3.5	Yes	18.2	16.5	8.9	6.6

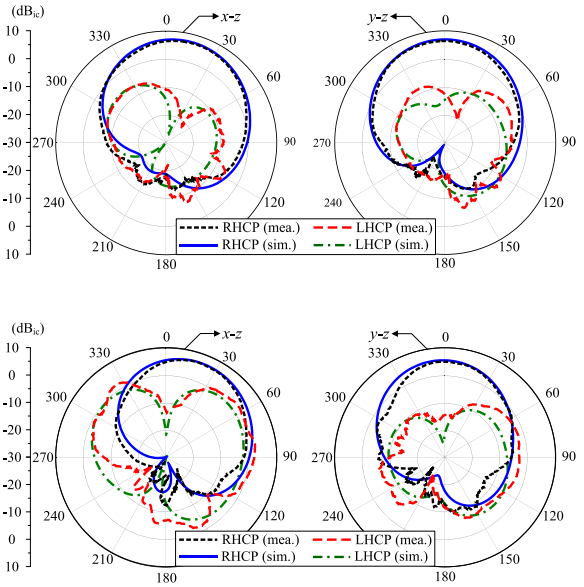

FIGURE 11. Simulated and measured gain radiation patterns at (a) 5.2 GHz and (b) 5.8 GHz.

the main beam is just about 1.6 dB. It is noted that the tilted pattern is also an issue in several reported designs [2]–[5], [11]. This issue may be overcome by designing with non-uniform parasitic elements to compensate for the effect of the branch line coupler, which is subjected for future investigation.

Finally, Table 1 shows a performance comparison among the dual-CP antennas. In this Table, the BW specified by isolation level should also cover the AR BW and impedance matching BW. It is apparent that the strong features of the proposed antenna are wide operating BW with high isolation while possessing a compact footprint and a low profile. Although the designs in [10], [22] have smaller footprints, their operating BW is significantly smaller than that of the proposed design. Slightly wider BW and higher gain can be achieved in [12, 13], but these designs have larger dimension and higher profile in comparison with the proposed antenna.

VI. CONCLUSION

This paper presents a compact dual-CP antenna with wideband operation and good isolation characteristics. The antenna is first designed with a microstrip square patch that is orthogonally excited by a branch line coupler. With the use of the coupler, the desired sense of CP radiation can be adjusted by feeding the appropriate input port. For CP operation and inter-port isolation enhancements, an array of metallic plates is periodically added around the patch. An antenna prototype was fabricated and tested, which shows good agreement between measurement and simulation. The prototype exhibits wideband operation of 16.5% (5.0–5.9 GHz). Across this band, inter-port isolation greater than 15 dB and gain higher than 4.3 dBic are achieved.

REFERENCES

[1] K. P. Liolis, J. Gomez-Vilardebo, E. Casini, and A. I. Perez-Neira, "Statistical modeling of dual-polarized MIMO land mobile satellite channels," *IEEE Trans. Commun.*, vol. 58, no. 11, pp. 3077–3083, Nov. 2010.
[2] S. Chaudhuri, R. S. Kshetrimayum, and R. K. Sonkar, "High inter-port isolation dual circularly polarized slot antenna with split-ring resonator based novel metasurface," *AEU Int. J. Electron. Commun.*, vol. 107, pp. 146–156, Jul. 2019.
[3] R. Xu, J.-Y. Li, J. Liu, S.-G. Zhou, Z.-J. Xing, and K. Wei, "A design of dual-wideband planar printed antenna for circular polarization diversity by combining slot and monopole modes," *IEEE Trans. Antennas Propag.*, vol. 66, no. 8, pp. 4326–4331, Aug. 2018.
[4] R. Xu, J.-Y. Li, J.-J. Yang, K. Wei, and Y.-X. Qi, "A design of U-Shaped slot antenna with broadband dual circularly polarized radiation," *IEEE Trans. Antennas Propag.*, vol. 65, no. 6, pp. 3217–3220, Jun. 2017.
[5] D. S. Chandu and S. S. Karthikeyan, "A novel broadband dual circularly polarized microstrip-fed monopole antenna," *IEEE Trans. Antennas Propag.*, vol. 65, no. 3, pp. 1410–1415, Mar. 2017.
[6] L. Xu, W. Lu, C. Yuan, and L. Zhu, "Dual circularly polarized loop antenna using a pair of resonant even-modes," *Int. J. RF Microw. Comput.-Aided Eng.*, vol. 29, no. 6, Jun. 2019, Art. no. e21703.
[7] G.-L. Wu, W. Mu, G. Zhao, and Y.-C. Jiao, "A novel design of dual circularly polarized antenna fed by L-strip," *Prog. Electromagn. Res.*, vol. 79, pp. 39–46, 2008.
[8] A. Narbudowicz, X. Bao, and M. J. Ammann, "Dual circularly-polarized patch antenna using even and odd feed-line modes," *IEEE Trans. Antennas Propag.*, vol. 61, no. 9, pp. 4828–4831, Sep. 2013.
[9] C. Zhang, X. Liang, X. Bai, J. Geng, and R. Jin, "A broadband dual circularly polarized patch antenna with wide beamwidth," *IEEE Antennas Wireless Propag. Lett.*, vol. 13, pp. 1457–1460, 2014.
[10] X.-Z. Lai, Z.-M. Xie, and X.-L. Cen, "Design of dual circularly polarized antenna with high isolation for RFID application," *Prog. Electromagn. Res.*, vol. 139, pp. 25–39, 2013.
[11] J. Wu, H. Yang, and Y.-Z. Yin, "Dual circularly polarized antenna with suspended strip line feeding," *Prog. Electromagn. Res. C*, vol. 55, pp. 9–16, 2014.
[12] C.-X. Mao, S. S. Gao, Y. Wang, and J. T. Sri Sumantyo, "Compact broadband dual-sense circularly polarized microstrip Antenna/Array with enhanced isolation," *IEEE Trans. Antennas Propag.*, vol. 65, no. 12, pp. 7073–7082, Dec. 2017.

[13] W. Yang, Q. Meng, W. Che, L. Gu, and Q. Xue, "Low-profile wideband dual-circularly polarized metasurface antenna array with large beamwidth," *IEEE Antennas Wireless Propag. Lett.*, vol. 17, no. 9, pp. 1613–1616, Sep. 2018.
[14] S. Liu, D. Yang, and J. Pan, "A low-profile broadband dual-circularly-polarized metasurface antenna," *IEEE Antennas Wireless Propag. Lett.*, vol. 18, no. 7, pp. 1395–1399, Jul. 2019.
[15] Y. Cai, Y. Zhang, Z. Qian, W. Cao, and S. Shi, "Compact wideband dual circularly polarized substrate integrated waveguide horn antenna," *IEEE Trans. Antennas Propag.*, vol. 64, no. 7, pp. 3184–3189, Jul. 2016.
[16] K. Kumar, S. Dwari, and M. K. Mandal, "Broadband dual circularly polarized substrate integrated waveguide antenna," *IEEE Antennas Wireless Propag. Lett.*, vol. 16, pp. 2971–2974, 2017.
[17] X.-Z. Lai, Z.-M. Xie, Q.-Q. Xie, and X.-L. Cen, "A dual circularly polarized RFID reader antenna with wideband isolation," *IEEE Antennas Wireless Propag. Lett.*, vol. 12, pp. 1630–1633, 2013.
[18] P. Squadrito, S. Zhang, and G. F. Pedersen, "X-band dual circularly polarized patch antenna with high gain for small satellites," *IEEE Access*, vol. 7, pp. 74925–74930, 2019.
[19] Y. He, C. Gu, H. Ma, J. Zhu, and G. V. Eleftheriades, "Miniaturized circularly polarized Doppler radar for human vital sign detection," *IEEE Trans. Antennas Propag.*, vol. 67, no. 11, pp. 7022–7030, Nov. 2019.
[20] Y.-K. Jung and B. Lee, "Dual-band circularly polarized microstrip RFID reader antenna using metamaterial branch-line coupler," *IEEE Trans. Antennas Propag.*, vol. 60, no. 2, pp. 786–791, Feb. 2012.
[21] Q. Luo, L. Zhang, and S. Gao, "Wideband multilayer dual circularly-polarised antenna for array application," *Electron. Lett.*, vol. 51, no. 25, pp. 2087–2089, Dec. 2015.
[22] R. Ferreira, J. Joubert, and J. W. Odendaal, "A compact dual-circularly polarized cavity-backed ring-slot antenna," *IEEE Trans. Antennas Propag.*, vol. 65, no. 1, pp. 364–368, Jan. 2017.
[23] D. M. Pozzar, *Microwave Engineering*, 4th ed. Hoboken, NJ, USA: Wiley, 2012.

HUY HUNG TRAN received the B.S. degree in electronics and telecommunications from the Hanoi University of Science and Technology, Hanoi, Vietnam, in 2013, the M.S. degree from Ajou University, Suwon, South Korea, in 2015, and the Ph.D. degree from Dongguk University, Seoul, South Korea.

His current research interests include circularly polarized antennas, high-gain antennas, metamaterial-based antennas, and reconfigurable antennas.

NGHIA NGUYEN-TRONG (Member, IEEE) received the Ph.D. degree in electrical engineering from The University of Adelaide, Adelaide, SA, Australia, in 2017.

He is currently with The University of Queensland, Brisbane, QLD, Australia, as a Postdoctoral Research Fellow. His current research interests include leaky-wave antennas, monopolar antennas, Fabry–Perot antennas, and reconfigurable antennas.

Dr. Nguyen-Trong was one of the recipients of the Best Student Paper Award from the IWAT in 2014, IEEE MTT-S NEMO in 2015, and ASA Conferences in 2017, and the Best Paper Award from the AMS Conference in 2018 and 2020. He serves as the Technical Chair of the Australian Microwave Symposium (AMS). He was selected as a Top Reviewer for the IEEE Antennas Wireless and Propagation Letters in 2018 and the IEEE Transactions on Antennas and Propagation (TAP) in 2019.

HYUN CHANG PARK (Member, IEEE) received the B.S. degree in electronics engineering from Seoul National University, Seoul, South Korea, in 1986, and the M.S. and Ph.D. degrees in electrical engineering from Cornell University, Ithaca, NY, USA, in 1989 and 1993, respectively.

From 1993 to 1995, he was with the Department of Electrical Engineering, University of Virginia, Charlottesville, as a Research Associate. In 1995, he joined the Faculty of Dongguk University, Seoul, South Korea, where he is currently a Professor with the Department of Electronics and Electrical Engineering. His research interests include RF energy harvesting, wideband/multi-band planar antennas, and reconfigurable antennas for various wireless applications.